Bioconjugate Chemistry

Article

pubs.acs.org/bc

New Fluorescent Labels with Tunable Hydrophilicity for the Rational Design of Bright Optical Probes for Molecular Imaging

Jutta Pauli,[†] Kai Licha,[‡] Janis Berkemeyer,[†] Markus Grabolle,[†] Monika Spieles,[†] Nicole Wegner,[‡] Pia Welker,[‡] and Ute Resch-Genger*[,†]

[†]BAM Federal Institute for Materials Research and Testing, Division 1.10 Biophotonics, Richard-Willstaetter-Strasse 11, D-12489 Berlin, Germany

[‡]mivenion GmbH, Robert-Koch-Platz 4, D-10115 Berlin, Germany

ABSTRACT: The rational design of bright optical probes and dye−biomolecule conjugates in the NIR-region requires fluorescent labels that retain their high fluorescence quantum yields when bound to a recognition unit or upon interaction with a target. Because hydrophilicity-controlled dye aggregation in conjunction with homo-FRET presents one of the major fluorescence deactivation pathways in dye−protein conjugates, fluorescent labels are required that enable higher labeling degrees with minimum dye aggregation. Aiming at a better understanding of the factors governing dye−dye interactions, we systematically studied the signal-relevant spectroscopic properties, hydrophilicity, and aggregation behavior of the novel *x*S-IDCC series of symmetric pentamethines equipped with two, four, and six sulfonic acid groups and selected conjugates of these dyes with IgG and the antibody cetuximab (ctx) directed against the cancer-related epidermal growth factor (EGF) receptor in comparison to the gold standard Cy5.5. With 6S-IDCC, which displays a molar absorption coefficient of 190 000 M^{-1} cm^{-1} and a fluorescence quantum yield (Φ_f) of 0.18 in aqueous media like PBS and nearly no aggregation, we could identify a fluorophore with a similarly good performance as Cy5.5. Bioconjugation of 6S-IDCC and Cy5.5 yielded highly emissive targeted probes with comparable Φ_f values of 0.29 for a dye-to-protein (D/P) ratio <1 and a reduced number of protein-bound dye aggregates in the case of 6S-IDCC. Binding studies of the ctx conjugates of both dyes performed by fluorescence microscopy and FACS revealed that the binding strength between the targeted probes and the EGF receptor at the cell membrane is independent of D/P ratio. These results underline the importance of an application-specific tuning of dye hydrophilicity for the design of bright fluorescent reporters and efficient optical probes. Moreover, we could demonstrate the potential of fluorescence spectroscopy to predict the size of fluorescence signals resulting for other fluorescence techniques such as FACS.

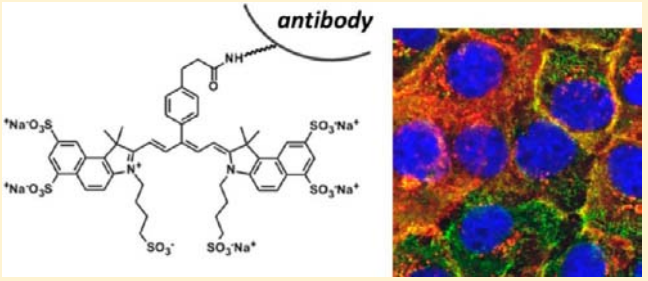

INTRODUCTION

Fluorescence measurements in the near-infrared (NIR) present a powerful tool to investigate biological materials due to the high sensitivity of fluorescence and the low autofluorescence in this spectral region.[1,2] This enables, for example, the direct investigation of diseases on a molecular level *in vitro* and *in vivo* with nonionizing radiation and comparatively simple and inexpensive instrumentation.[3] At the core of such measurements are bright fluorescent reporters with NIR absorption and emission,[4−8] suitable reporter−biomolecule conjugation chemistries[9,10] and signaling schemes,[4,11−14] analytical techniques for the characterization of the resulting bioconjugates,[15,16] and novel instrumentation and detection techniques.[17,18] Although exciting fluorescent nanomaterials such as semiconductor quantum dots and dye-labeled or doped nanoparticles reveal superior optical properties compared with conventional small organic dyes[4,7] and enable the straightforward combination of different imaging modalities or multiplexed detection strategies,[11,19] their use is still hampered by unresolved issues of toxicology. Moreover, the reproducible production of these materials still presents a challenge. This is similarly true for their analytical characterization.[4,20] This renders small organic dyes the presently most widely used fluorescent reporters because methods for their bioconjugation and the characterization of the resulting bioconjugates are meanwhile established.

The vast majority of NIR chromophores utilized until now for the design of optical imaging agents are cyanine dyes,[17,21−26] typically symmetric indocarbocyanines such as the Cy dyes Cy5, 5.5, 7, and 7.5. Increasingly, also asymmetrically substituted polymethines like the Dy dyes are employed that are available with different substitution patterns and varying degrees of hydrophilicity. Searching for bright fluorescent labels that retain their favorable fluorescence properties also in dye−biomolecule conjugates, we spectroscopically investigated many of these fluorophores and utilized

Received: January 17, 2013
Revised: May 6, 2013
Published: June 11, 2013

dx.doi.org/10.1021/bc4000349 | *Bioconjugate Chem.* 2013, 24, 1174−1185

them for the synthesis of targeted optical probes for *in vitro* and *in vivo* biomarker imaging.[27−31] Other alternatives include squaraine dyes[32,33] and porphyrins (free base dyes and metalloporphyrins). Depending on the central metal ion, metalloporphyrins can be also employed for the design of stimuli-responsive probes, for example, for oxygen sensing.[34,35]

Despite the large toolbox of fluorescent labels to choose from, there is still extensive research dedicated to the rational design of new fluorescent labels with improved performance. Of special interest are stable and nontoxic NIR-emissive fluorophores with an enhanced brightness, that is, a high fluorescence quantum yield (Φ_f) and a high molar absorption coefficient under application-relevant conditions in aqueous media and attached to a biomolecule. The latter is closely linked to the minimization of fluorescence-diminishing dye aggregation in water and for targeted optical probes, also on the biomolecule. Dye aggregation leads to considerable changes in the absorption spectrum including the appearance of new absorption bands. The spectral position and shape of these new bands depend on the orientation of the interacting transition dipole moments of the dye molecules,[36−38] with blue-shifted absorption bands being typical for so-called H-aggregates and red-shifted narrowed bands for so-called J-aggregates. H-aggregates that typically absorb in a region where the monomer itself absorbs, are non- or barely emissive, whereas J-aggregates show an intense and narrow resonant emission. Minimization of dye aggregation in bioconjugates presents still a considerable challenge as underlined by spectroscopic studies of many currently used fluorescent reporters that all form nonemissive aggregates even at moderate dye-to-protein ratios even when equipped with up to four sulfonic acid groups or with sterically demanding substituents like *tert*-butyl groups.[31,39−43] To the best of our knowledge, the only example where all biomolecule-bound fluorophores equally contribute to the measured optical signal has been obtained with lanthanide chelates.[44] These fluorophores with their largely Stokes-shifted emission do not form aggregates and cannot undergo homo-FRET (FRET, Förster resonance energy transfer) yet require short wavelength excitation and display only very small molar absorption coefficients due to the forbidden nature of the optical transitions involved.

To overcome these challenges, we designed a new family of NIR dyes closely related to the Cy dyes, the *x*S-IDCC series shown in Figure 1. These dyes can be substituted at their benzoindole end groups with up to six sulfonate groups. Moreover, in contrast to the Cy and Dy dyes, subsequent bioconjugation occurs not via a substituent like a NHS ester group attached to one of the aromatic end groups of the polymethine chain but via a phenyl substituent in the middle of the polymethine chain. This straightforward and synthetically not very demanding design concept can be easily extended to longer wavelength absorbing and emitting dyes and to stimuli-responsive molecules.

Here, we present a systematic study of the spectroscopic properties of these new fluorophores in different solvents and conjugated to two antibodies in comparison to the spectrally matching gold standard Cy5.5 containing four sulfonate groups and to the asymmetric polymethine Dy682 previously investigated by us that is equipped with three sulfonate groups.[43] For the bioconjugation studies, we used IgG as a model system to enable the comparison with other literature systems,[25,45,46] and the monoclonal antibody cetuximab (ctx) directed against the cancer-related EGF receptor. In addition to

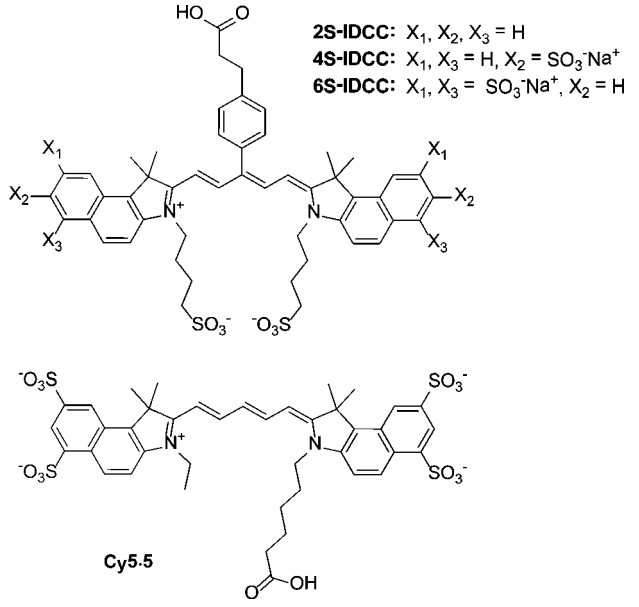

Figure 1. Chemical structures of the cyanine dyes 2S-, 4S-, and 6S-IDCC: top, *x*S-IDCC series with *x* denoting the number of sulfonate groups; bottom, Cy5.5.

spectroscopic studies, the performance of these targeted optical probes was also assessed in cellular binding studies using fluorescence microscopy and flow cytometry. The overall goals were here to identify new bright dyes for protein labeling and molecular imaging that preserve their favorable optical properties upon bioconjugation and to gain a deeper understanding of the relationship between dye hydrophilicity, the formation of dye aggregates in bioconjugates, and dye-induced protein aggregation for the rational design of the next generation of labeling reagents with an integrated sensor function, for example, for pH or reactive oxygen species (ROS).

EXPERIMENTAL PROCEDURES

Materials. The three dyes from the *x*S-IDCC series, 2S-IDCC, 4S-IDCC, and 6S-IDCC, with *x* referring to the number of sulfonate groups attached to both indocarbocyanine end groups of these symmetric cyanines were provided by mivenion GmbH (Berlin, Germany). Dye purity was determined to 99.9% for 2S-IDCC, 94% for 4S-IDCC, and 90% for 6S-IDCC using high-performance liquid chromatography (HPLC) as described in the following section. Cy5.5 Mono NHS ester, which was hydrolyzed to yield the corresponding acid used for the spectroscopic studies, and Cy5.5 monomaleimide employed for IgG and ctx labeling were purchased from GE Healthcare (Amersham, United Kingdom). 6S-IDCC monomaleimide was synthesized by mivenion GmbH (Berlin, Germany). 2-Iminothiolane[47] was obtained from Sigma Aldrich. Oxazine 1 employed as fluorescence quantum yield standard was purchased from Lambda Physik GmbH (Goettingen, Germany).[48] IgG from human serum (reagent grade, salt free, lyophilizate) and ethanol (spectroscopic grade) were purchased from Sigma Aldrich. Cetuximab was isolated from the market solution (Erbitux solution for injection 5 mg/mL, Merck KGaA) by ultrafiltration and lyophilization. Phosphate buffer solution (PBS, stock solution: 1.37 M NaCl, 27 mM KCl, 100 mM Na_2HPO_4, 20 mM KH_2PO_4) was obtained from Carl Roth + co. KG (Karlsruhe, Germany). Typically, this stock solution

dx.doi.org/10.1021/bc4000349 | *Bioconjugate Chem.* 2013, 24, 1174−1185

was diluted 10 times. Bovine serum albumin (BSA; fraction V) was purchased from Merck KgaA (Darmstadt, Germany).

Preparation of 6S-IDCC and Cy5.5 Dye−Antibody Conjugates (IgG−Dye and ctx−Dye). For antibody labeling via preactivation with iminothiolane, 6S-IDCC was modified with 1-(2-aminoethyl)maleimide to yield 6S-IDCC maleimide, and in the case of Cy 5.5, the commercialized maleimide was used. Generally, 8 mg of the antibody was dissolved in 1100 μL of PBS (pH 7.4) followed by addition of a solution of 2-iminothiolane in PBS (1.5−3.0 mg/mL). After 30 min of gentle shaking, 6S-IDCC maleimide or Cy5.5 maleimide was added from a stock solution of the respective dye in PBS (concentration of 3−8 mg/mL). The ratio of 2-iminothiolane and the reactive dye used equaled 2, 5, and 10 molecular equivalents (mol equiv) for 2-iminothiolane/6S-IDCC and 3 and 5 mol equiv for 2-iminothiolane/Cy5.5 maleimide. The reaction mixtures were shaken for 3 h at room temperature. Purification was performed with column chromatography using Sephadex columns (NAP10, Amersham) and PBS as eluent. The absence of unbound dye in the conjugate solutions was confirmed by size exclusion HPLC (MAbPac SEC-1 column, eluent PBS pH 6.6) and by thin layer chromatography (RP-C18 TLC). The resulting solutions of the dye−biomolecule conjugates were then analyzed with respect to their dye-to-protein (D/P) ratio.

HPLC Measurements. Dye purity and dye hydrophilicity were determined with high-performance liquid chromatography (HPLC). The measurements were performed at T = 296 K and a pressure of 200 bar with a HPLC system 1200 from Agilent equipped with a diode array detector (detection at 674 nm) and a fluorescence detector and Ultrasep ESPHEN 250 mm × 3 mm column from SEPSERV, Germany. As solvent, we used a mixture of water and acetonitrile containing ammonium acetate (10 mM) (linear gradient from polar (90% water) to less polar (90% CH_3CN) in a time range of 22 min) and a flow rate of 0.4 mL/min.

For purity analysis of xS-IDCCs, we used the absorbances measured at 674 nm and a 100% method. Moreover, the retention times of xS-IDCC series, Cy5.5, and Dy682 previously studied by us[43] were determined as a measure for the (relative) hydrophilicity of these dyes. Under these conditions, short retention times imply a high hydrophilicity of the eluted species.

Absorption and Fluorescence Measurements. The absorption spectra were recorded on a CARY 5000 spectrophotometer (Varian Inc., Palo Alto, USA) using 1 cm quartz cells. The absorption spectra of the xS-IDCC dyes and Cy5.5 and their antibody conjugates were determined in duplicate in ethanol (dyes only), in PBS (1×10^{-6} mol/L, pH 7.8), and in PBS containing 5% (w/w) BSA (PBS/BSA). For selected samples, measurements were also performed in water (aqua dest). The molar absorption coefficients of each dye at the dye's absorption maximum, $\varepsilon(\lambda_{max})$, was determined from three independent measurements of the absorption spectra of single diluted stock solutions in ethanol, PBS, and BSA/PBS. For the aggregation studies, quartz cells with optical pathlengths varying from 0.001 to 1 cm were employed. Measurements with these microcuvettes were carried out with an OMEGA spectrophotometer (Bruins Instruments). Fluorescence measurements were performed with a calibrated Spectronics Instruments 8100 (Westbury, USA) spectrofluorometer (T-type design; solely use of NIR emission channel here) equipped with Glan Thompson polarizers in the excitation and the emission channel (set to 0° and 54.7°).[49] Typically, the emission spectra of the solutions of the free fluorophores were determined in 1 cm-quartz cells in duplicate. Typically, the samples were excited at the vibronic shoulder of the dye's longest wavelength absorption band using absorbances of 0.02 to 0.06 (equaling dye concentrations between 1×10^{-6} and 1×10^{-7} mol/L) to minimize inner filter effects and reabsorption. The fluorescence spectra of the dye−antibody conjugates in PBS solutions were measured in duplicate in 4 mm cuvettes (Hellma, type 108F-QS) using an excitation wavelength of 665 nm and absorbances of the samples of 0.02 to 0.06. For each sample, also the excitation spectra were recorded that represent the absorption spectra of the emitting species.

For each compound−solvent pair, the fluorescence quantum yields (Φ_f) were determined in duplicate using dye and standard solutions freshly prepared by dilution of stock solutions (typically, dye concentration of 100×10^{-6} mol/L, stored in the refrigerator at 4 °C in the dark). The Φ_f values of the nonconjugated and the antibody-bound dyes were calculated from integrated, blank, and spectrally corrected emission spectra (wavelength scale; prior to integration multiplication with λ)[1,49] relative to the standard oxazine 1 dissolved in ethanol (Φ_f = 0.143) using the following formula:

$$\Phi_{f,x} = \Phi_{f,st} \frac{F_x}{F_{st}} \frac{f_{st}(\lambda_{ex})}{f_x(\lambda_{ex})} \frac{{n_x}^2}{{n_{st}}^2} \quad (1)$$

Here, $f(\lambda_{ex})$ is the absorption factor at the excitation wavelength λ_{ex}, F is the integral emission intensity, that is, the area under the blank and spectrally corrected emission spectrum on a wavelength scale, and n is the refractive index of the solvent(s) used. The subscripts x and st denote sample and standard. Typical instrument-related relative measurement uncertainties as derived from previous experiments are less than ±6% (for $0.9 > \Phi_f > 0.1$).[48,50]

Determination of the Dimerization Constants and the Amount of Monomeric Dyes in the Dye Bioconjugates. The dimerization constants and the amount of monomeric dyes in the bioconjugates resulting in varying dye-to-protein ratios in the reaction mixtures were determined as previously described by us for the dyes Dy676, Dy678, Dy681, and Dy682, respectively.[43]

Dye-to-Protein (D/P) Ratio of the Dye Bioconjugates. The D/P ratio was calculated according to eq 2.[51,52]

$$\mathrm{D/P} = \frac{c_D}{c_P} = \frac{\varepsilon_{P,280} A_{D,680}}{\varepsilon_D (A_{280} - k A_{D,680})} \quad (2)$$

The molar absorption coefficients of the proteins at 280 nm ($\varepsilon_{P,280}$) were determined to be 190 000 L mol^{-1} cm^{-1} for IgG and 170 000 L mol^{-1} cm^{-1} for cetuximab in PBS. The molar absorption coefficients of the dyes used were 197 000 L mol^{-1} cm^{-1} (6S-IDCC; 680 nm) and 178 000 L mol^{-1} cm^{-1} (Cy5.5; 680 nm) in PBS. The absorbance of the dye at 280 nm is considered by the factor k that equals the ratio of the dye absorbances at 280 and 680 nm; k was calculated to be 0.10 for 6S-IDCC and 0.11 for Cy5.5, respectively.

Cell Studies. The epithelial human cancer cell lines A549 and A431 were routinely propagated as follows: DEMEM medium with 10% fetal calf serum, 2% glutamine, and penicillin/streptomycin (all from PAN Biotech) was added to the culture dish. The cells were seeded into the medium at a concentration of 1×10^5 cells/mL, cultured at 37 °C with 5%

Table 1. Spectroscopic Properties of the *x*S-IDCC Serie in Ethanol, PBS, and PBS/BSA in Comparison to Cy5.5[a]

dye	solvent	λ_{abs}, nm	λ_{em}, nm	Stokes shift, nm (cm^{-1})	ε, L mol^{-1} cm^{-1}	Φ_f	B, L mol^{-1} cm^{-1}
2S-IDCC	ethanol	686	710	24 (493)	180 000	0.26	49 000
2S-IDCC	PBS	679	702	23 (483)	*b*	0.10	*b*
2S-IDCC	PBS/BSA	702	718	16 (317)	158 000	0.38	60 000
4S-IDCC	ethanol	690	712	22 (448)	189 000	0.35	66 000
4S-IDCC	PBS	681	704	23 (480)	179 000	0.16	29 000
4S-IDCC	PBS/BSA	697	712	15 (302)	158 000	0.36	57 000
6S-IDCC	ethanol	686	708	22 (453)	190 000	0.35	67 000
6S-IDCC	PBS	676	696	20 (425)	197 000	0.18	35 000
6S-IDCC	PBS/BSA	685	702	17 (354)	170 000	0.39	66 000
Cy5.5	ethanol	684	708	24 (496)	167 000	0.33	55 000
Cy5.5	PBS	675	692	17 (364)	178 000	0.28	50 000
Cy5.5	PBS/BSA	681	700	19 (399)	146 000	0.43	63 000

[a]Properties presented are maxima of the main absorption (λ_{abs}) and emission (λ_{em}) bands, Stokes shift (in nm and in cm^{-1}), molar absorption coefficients, ε, at the absorption maximum, fluorescence quantum yields (Φ_f), and brightness B ($B = \varepsilon(\lambda_{max}) \times \Phi_f$). [b]Not determined.

CO_2, and divided 1:10 twice a week. The cells were seeded at a concentration of 5×10^4 cells/mL in a 24-well culture plate on glass coverslips (Sigma), and cultured for 24 h at 37 °C. Then, the cells were incubated with a medium containing 5 μg/mL antibody conjugates for 45 min at 37 °C. Afterward, the cells were fixed with cold acetone, rinsed, and covered with Alexa Fluor 488 Phalloidin (1:300, Molecular Probes) or a rabbit polyclonal anti-ZO-1 antibody (abcam) and a Cy2-labeled anti-rabbit secondary antibody (Dianova). 4,6-Diamidino-2-phenylindole (DAPI, abcam) was used for nuclear counterstaining. Image acquisition of cellular fluorescence was performed using a confocal microscope LSM 5 Exiter (Zeiss) equipped with a laser diode (excitation at 405−425 nm), an Ar^+-laser (excitation at 456, 488, and 514 nm), and a HeNe-laser (excitation at 633 nm). All images were taken at the same exposure time of 200 ms to enable the comparison of the measured fluorescence signals. For fluorescence activated cell sorting (FACS), 2×10^5 viable cells/mL were cultured in 24-well plates for 24 h at 37 °C. Subsequently, the cells were incubated with normal culture medium or medium containing 5 μg/mL antibody conjugate for 45 min. The cells were washed with PBS, detached with 200 μL/well of accutase (PAA), and washed twice with PBS. The cells were fixed with 500 μL of 3% paraformaldehyde for 10 min at 4 °C, stopped with 2 mL of PBS, and centrifuged at 250*g* for 10 min at 4 °C. The supernatants were removed, and the cells were suspended in 200 μL of PBS with 0.5% bovine serum albumin (Roth). The fixed cells were kept at 4 °C until analysis with a FACS Calibur instrument SL4 (Becton-Dickinson). For the FACS analysis, excitation was at 633 nm and a bandpass filter of 661 ± 8 nm for the emission channel was used.

RESULTS AND DISCUSSION

Spectroscopic Properties of *x*S-IDCC. The signal-relevant spectroscopic properties of the *x*S-IDCC dyes obtained in ethanol, PBS, and 5% (w/w) BSA (PBS/BSA) modeling body fluid are summarized in Table 1. As to be expected from the similar structure of the *x*S-IDCC dyes and Cy5.5, their absorption and emission spectra closely match in ethanol and PBS and, hence, also their Stokes shifts. Only in PBS/BSA, the spectral position of the absorption and emission bands of the *x*S-IDCC dyes are clearly affected by the number of the sulfonate groups, with an increase in x resulting in a continuous blue shift in absorption and emission and thus, in a closer match between the corresponding spectra in PBS/BSA, PBS, and ethanol. The size of these spectral shifts in the presence of BSA seems to correlate with the expected binding strength between the dye and BSA that typically increases with decreasing hydrophilicity,[53] see also next section. As follows from Table 1, the molar absorption coefficients ε and the Φ_f values of the *x*S-IDCC fluorophores depend on solvent and on the number of the sulfonate groups. The highest ε values are observed in ethanol, followed by PBS, and PBS/BSA. We did not attempt to determine the molar absorption coefficient of 2S-IDCC in PBS because of its pronounced aggregation tendency in this solvent. With values of 0.35 to 0.39, the fluorescence quantum yields of 6S-IDCC and 4S-IDCC are comparable in ethanol and PBS/BSA and exceed the Φ_f values found for these dyes in PBS by a factor of ca. 2, as well as the Φ_f values obtained for 2S-IDCC in ethanol and in PBS. The Φ_f values measured in PBS always match the Φ_f values in bidistilled water (data not shown), thereby excluding a possible influence of ionic strength and dissolved salts.

The molar absorption coefficients of the *x*S-IDCC fluorophores exceed those of Cy5.5 in all solvents studied (see Table 1), whereas their Φ_f values fall below the Φ_f values of Cy5.5 in PBS and PBS/BSA. In ethanol, however, the Φ_f values of 6S-IDCC, 4S-IDCC, and Cy5.5 are comparable. As a measure for dye performance, we determined the brightness values, B, from the molar absorption coefficients, ε, at the dye's absorption maximum, λ_{max}, and the fluorescence quantum yield ($B = \varepsilon(\lambda_{max}) \times \Phi_f$). For spectrally matching dyes like the *x*S-IDCC dyes, Cy5.5, and Dy682, this should reflect the desired correlation with the observable signals, although we did not use the ε value at the excitation wavelength. Moreover, most dye manufacturers and researchers use a similar approach.[54] Despite its higher molar absorption coefficient, the brightness of the most favorable dye of the *x*S-IDCC serie, 6S-IDCC, is still inferior to that of Cy5.5 in PBS, yet it exceeds the brightness of this gold standard in PBS/BSA and in ethanol. Nevertheless, 6S-IDCC clearly outperforms, for example, the most efficient dye from the Dy68*x* series, Dy682 (ε = 110 000 L mol^{-1} cm^{-1}; Φ_f = 0.2; B = 22 000 L mol^{-1} cm^{-1}) and other fluorescent labels frequently used for molecular imaging.

Dye Hydrophilicity. The hydrophilicity of the *x*S-IDCC dyes and Cy5.5 (four SO_3^- groups), as well as Dy682 (three SO_3^- groups) previously studied by us together with other Dy dyes [43] were compared based upon the retention times obtained by HPLC measurements under identical conditions (same column, eluent gradient, flow rate, temperature, and pressure). With this procedure, retention times of 10.4, 11.6,

dx.doi.org/10.1021/bc4000349 | Bioconjugate Chem. 2013, 24, 1174−1185

12.4, 13.5, and 20.0 min were determined for 6S-IDCC, Cy5.5, 4S-IDCC, Dy682, and 2S-IDCC, respectively, thereby revealing the following trend with respect to increasing hydrophilicity: 2S-IDCC (20.0 min) < Dy682 (13.5 min) < 4S-IDCC (12.4 min) < Cy5.5 (11.6 min) < 6S-IDCC (10.4 min). Obviously, the main factor governing dye hydrophilicity is the number of sulfonate groups at the chromophore. As to be anticipated, 6S-IDCC with the highest number of sulfonate groups exhibits the highest hydrophilicity. The slightly increased hydrophilicity of Cy5.5 compared with 4S-IDCC, which comprises the same number of sulfonate and carboxylic acid groups, is tentatively ascribed to the phenyl substituent in the polymethine chain of 4S-IDCC.

Aggregation Studies and Dimerization Constants. The aggregation tendency of the *x*S-IDCC series in PBS and, interestingly, also the type of aggregates formed are controlled by the number of sulfonate groups and the dye hydrophilicity. As follows from the area-normalized absorption spectra (equaling the concentration-weighted absorbances for different dye concentrations)[55] shown in Figure 2, the most hydrophobic

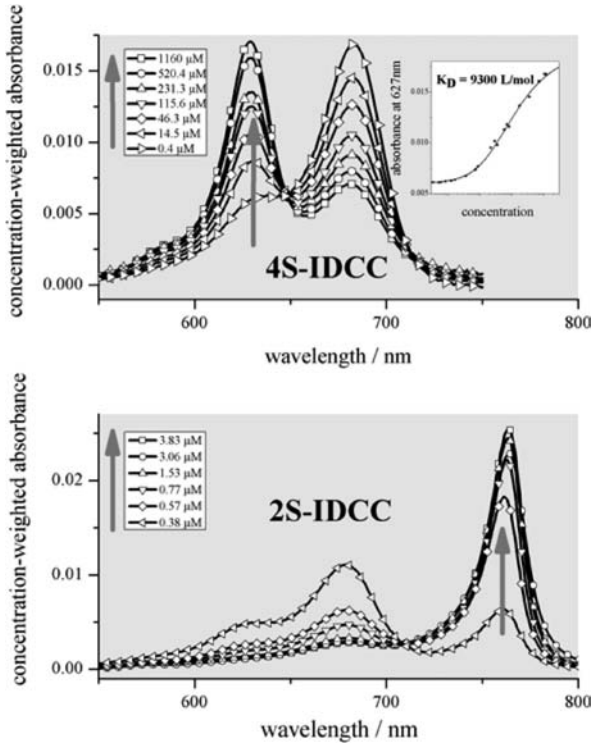

Figure 2. Concentration-weighted absorption spectra of 4S-IDCC (upper panel) and 2S-IDCC (lower panel) measured at different dye concentrations between 1.16×10^{-3} and 0.4×10^{-6} mol/L (4S-IDCC) or between 3.83×10^{-6} and 0.38×10^{-6} mol/L (2S-IDCC) in PBS, respectively.

dye, 2S-IDCC (lower panel), forms aggregates already at very low dye concentrations of 3.8×10^{-6} mol/L. Interestingly, for this dye, an increase in dye concentration does not lead to the typically observed blue shift in absorption as displayed by the vast majority of cyanine-type fluorescent labels like the Dy dyes Dy68*x* and Dy67*x* used in bioanalysis and molecular imaging.[25,31,36,46,51,56−58] The spectral position and shape of this newly formed absorption band suggests the formation of J-type aggregates for 2S-IDCC (see Figure 2, lower panel) and thus, a linear orientation of the interacting transition dipole moments.[36,37,59] The area-normalized absorption spectra of 2S-IDCC do not reveal a clear isosbestic point, which may point to the formation of different types of aggregates. Moreover, the absorption maximum of the J-aggregates shifts between 764 and 761 nm with varying dye concentration, suggesting slightly different orientations of the fluorophore molecules [60] or different numbers of fluorophores in the aggregates.[59,61] This hampers the determination of an aggregation constant from concentration-dependent changes in the absorbance.

Contrary to 2S-IDCC, 4S-IDCC forms the commonly observed H-type dimers as indicated by the blue-shifted absorption band with increasing dye concentration (Figure 2, upper panel). The isosbestic points (at 648 and 715 nm) resulting for the area-normalized absorption spectra provide a clear hint of the exclusive formation of dimers.[38] From these data, we derived a dimerization constant, K_D, of 9.3×10^3 L/mol (see plot of the concentration-dependent changes in the absorbance at 627 nm, that is, the dimer absorption band; inset in Figure 2, upper panel). This dimerization constant, which is of the same order of magnitude as found for other cyanine dyes, exceeds the K_D value found for Dy682 (K_D of 2×10^3 L/mol), and is comparable to that obtained for Dy678 (K_D of 8×10^3 L/mol).[43] The most hydrophilic dye of the *x*S-IDCC series, 6S-IDCC, barely aggregates at all in PBS even at very high dye concentrations, with dye aggregation starting at a concentration of 4×10^{-4} mol/L. Due to solubility problems at dye concentrations exceeding 2.5×10^{-3} mol/L, we could not determine a dimerization constant for this dye, but only estimate a dimerization constant from the few data points obtained assuming a similar shape of the concentration dependence of the absorbance as found for 4S-IDCC and other cyanine dyes. This yields a K_D value below 30 L/mol. These results, in conjunction with the favorable optical properties discussed in the previous section, hold great promise for the application of this dye as a fluorescent label for proteins and bioimaging applications.

Aggregation studies with Cy5.5 in PBS reveal the expected formation of H-type dimers. Similarly as for 6S-IDCC, due to solubility problems, we could only estimate the dimerization constant of Cy5.5 from the few data points obtained, yielding a K_D value between 150 and 300 L/mol. This clearly exceeds the value estimated for 6S-IDCC.

These studies also reveal the importance of different structural elements for dye aggregation and the orientation of the molecules in these aggregates. Possibly, the phenyl group in 2S-IDCC is oriented in a more planar fashion to the polymethine chain as the phenyl groups in 4S-IDCC and 6S-IDCC equipped with more sulfonic acid groups favoring electrostatic repulsion. The clarification of this hypothesis requires further systematic studies. This will be the subject of future research activities as well as the aggregation behavior of this dye on different biomolecules.

Dye−Antibody Conjugates. Considering 6S-IDCC to be the most promising fluorescent label of the *x*S-IDCC family, only conjugates of this dye with the nonbinding antibody IgG, often used as a model system for the assessment of label performance and as control in many fluorescence imaging studies, and the antibody cetuximab (ctx) targeting the EGF receptor were prepared using different D/P ratios and then spectroscopically investigated. For the evaluation of the performance of our new fluorescent reporter, also different conjugates of the gold standard Cy5.5 with IgG and ctx with comparable D/P ratios were synthesized. For the preparation of

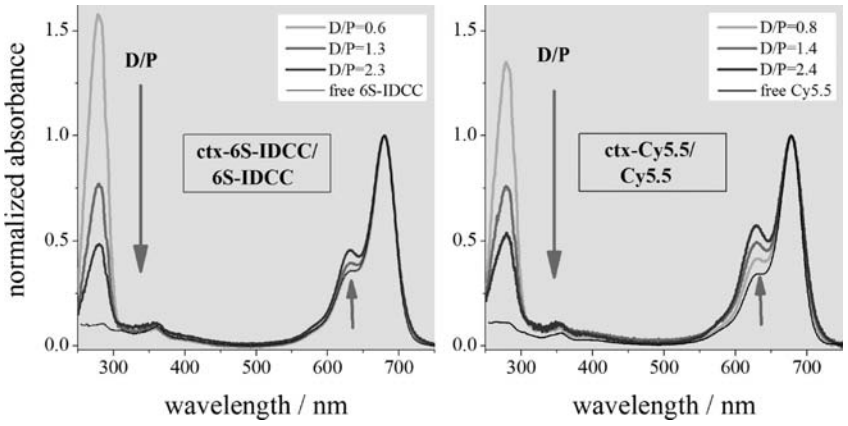

Figure 3. Normalized absorption spectra of ctx−6S-IDCC (left panel) and ctx−Cy5.5 (right panel) in PBS as function of D/P ratio in comparison to the absorption spectra of the corresponding free dyes.

Table 2. Fluorescence Quantum Yields and Maxima of the Main Absorption (λ_{abs}) and Emission (λ_{em}) Bands of the 6S-IDCC and Cy5.5 Conjugates in PBS with Different D/P Ratios

dye	D/P	λ_{abs}, nm	λ_{em}, nm	Stokes shift, nm (cm^{-1})	Φ_f	ε, L mol^{-1} cm^{-1}	B, L mol^{-1} cm^{-1}
IgG−6S-IDCC	0.6	679	702	23 (483)	0.29	197 000	57 130
IgG−6S-IDCC	1.3	679	702	23 (483)	0.26	197 000	51 220
IgG−6S-IDCC	2.7	679	702	23 (483)	0.17	197 000	33 490
ctx−6S-IDCC	0.6	679	700	21 (442)	0.29	197 000	57 130
ctx−6S-IDCC	1.3	679	700	21 (442)	0.25	197 000	49 250
ctx−6S-IDCC	2.3	679	700	21 (442)	0.20	197 000	39 400
IgG−Cy5.5	0.9	678	698	20 (423)	0.31	178 000	55 180
IgG−Cy5.5	1.3	678	698	20 (423)	0.29	178 000	51 620
IgG−Cy5.5	2.5	678	698	20 (423)	0.20	178 000	35 600
ctx−Cy5.5	0.8	678	696	18 (381)	0.30	178 000	53 400
ctx−Cy5.5	1.4	678	696	18 (381)	0.25	178 000	44 500
ctx−Cy5.5	2.4	678	697	19 (402)	0.16	178 000	28 480

the bioconjugates, we used the method of thiol incorporation via 2-iminothiolane followed by reaction with maleimido dyes, thereby allowing fast and mild labeling within 3 h. This statistical labeling method should not provide any preferences for particular sites in the antibody structure. Excess free dye could be quantitatively removed, as confirmed by size exclusion chromatographic and TLC analysis (data not shown). Figure 3 displays exemplarily the concentration-weighted absorption spectra of the ctx−6S-IDCC conjugates (left panel) and the ctx−Cy5.5 conjugates (right panel) in PBS in comparison to the spectra of the corresponding free dyes. The slight conjugation-induced red shifts of 5 nm in the dye absorption maxima of both fluorophores (see also Table 2) point to a less polar environment of the protein-bound dyes than in PBS solution. Interestingly, the bioconjugates of both 6S-IDCC and Cy5.5 show an increase in absorbance at the spectral position of the vibronic shoulder, the size of which increases with increasing D/P ratio. This indicates the formation of dye dimers on the protein surface, despite the minimum aggregation tendency observed for the free dyes in PBS solution. A similar behavior was observed for the IgG conjugates.

The amount of monomeric dyes in the ctx and IgG conjugates of 6S-IDCC and Cy5.5 as derived from the previously determined absorption spectra of the monomeric and dimeric fluorophores is depicted in Figure 4. As to be expected and observed for other dye−biomolecule conjugates, the fraction of monomeric dyes decreases in all cases with

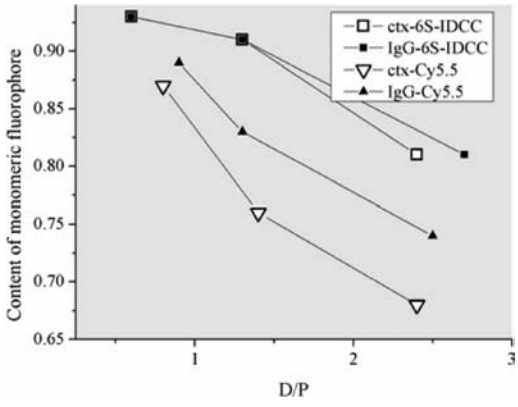

Figure 4. Content of monomeric 6S-IDCC and Cy5.5 in the corresponding ctx and IgG conjugates obtained for different D/P ratios. A fraction of 1.0 results for bioconjugates that contain solely the monomeric fluorophore.

increasing D/P ratio.[25,31,40,43,45,46] Although none of the bioconjugates studied contained solely the monomeric fluorophore (fraction of 1.0) even at very low D/P ratios, the found content of 0.96 for ctx−6S-IDCC and IgG−6S-IDCC are most likely the best values reported to date, emphasizing the excellent suitability of 6S-IDCC as protein label. For instance, for IgG−Dy682 with a D/P ratio of 0.7, we found a fraction of monomeric Dy682 of 0.85. These results underline that the hydrophilicity of the fluorescent label is the main factor

dx.doi.org/10.1021/bc4000349 | Bioconjugate Chem. 2013, 24, 1174−1185

controling the fraction of monomeric dyes in the bioconjugates. Moreover, also the antibody itself seems to affect dye dimerization as suggested by a comparison of the content of monomeric dye of the bioconjugates ctx–Cy5.5 and IgG–Cy5.5. In the case of more hydrophilic and more highly charged 6S-IDCC, the monomer fraction is more or less identical for both antibodies studied.

Fluorescence studies of these dye bioconjugates in PBS summarized in Table 2 reveal also small conjugation-induced red shifts in emission for 6S-IDCC (ctx, 6 nm; IgG, 4 nm) and Cy5.5, respectively. For typically used moderate dye labeling densities of D/P < 1.5, the fluorescence quantum yields of the 6S-IDCC and Cy5.5 conjugates are remarkably high independent of the antibody used, exceeding those of the corresponding free dye in PBS by a factor of almost 2 in the case of 6S-IDCC and equaling the Φ_f of the free dye for Cy5.5. Hence, although the fluorescence quantum yield of non-conjugated 6S-IDCC in PBS amounts only to 60% of the Φ_f of Cy5.5, the Φ_f values of their bioconjugates become comparable as highlighted in Figure 5 comparing the Φ_f values of the

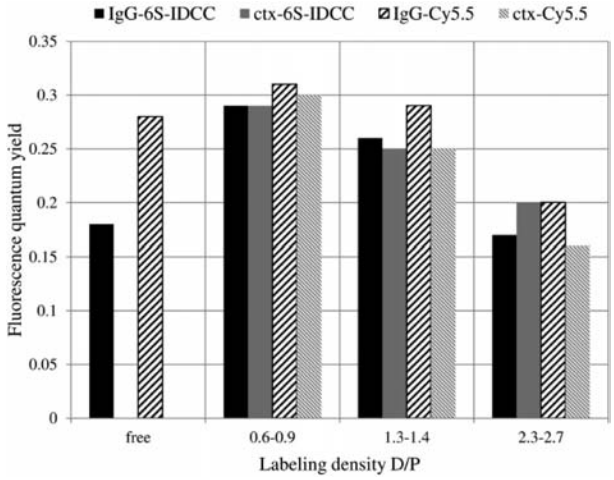

Figure 5. Fluorescence quantum yields of 6S-IDCC and Cy5.5 bioconjugates with three different labeling densities in PBS covering the following D/P ratios: (i) D/P < 1; (ii) 1 < D/P < 2; (iii) D/P > 2.

different 6S-IDCC and Cy5.5 antibody conjugates for different D/P ratios. Taking the higher molar absorption coefficient of 6S-IDCC into account, this should result in an enhanced brightness of bioconjugated 6S-IDCC compared with Cy5.5. This can yield improved detection sensitivities as desired, for example, for the detection and monitoring of metastases. At higher labeling densities of D/P > 2 (see Table 2 and Figure 5), the fluorescence quantum yields of both dyes are diminished, with the minimum Φ_f found for 6S-IDCC bioconjugates matching that of the nonconjugated dye of 0.18. In the case of Cy5.5, the Φ_f values of bioconjugates with D/P > 2 are 40% lower than that of free Cy5.5. The strong fluorescence enhancement observed for antibody conjugates of 6S-IDCC at low and moderate D/P ratios, which is in agreement with the fluorescence behavior of this fluorophore in PBS/BSA (see Table 1), is ascribed to bioconjugation-induced chromophore rigidization, thereby reducing the main nonradiative decay process active in such cyanines, cis–trans isomerization, possibly in conjunction with a reduced polarity of the dye microenvironment.[25,62] Interestingly, although the fluorescence of Cy5.5 is also enhanced in the presence of BSA (see Table 1), this is not the case upon bioconjugation. Whether this points to a different orientation of this fluorophore on the biomolecule surface, for example, due to the different length or position of attachment of the linker at the chromophore or the different dye charge/hydrophilicity can be only speculated. In agreement with the conjugation-induced changes in absorption (see Figure 2), the loss in fluorescence at higher D/P ratios is ascribed to dye dimerization and homo-FRET between protein-bound monomeric dyes and dimerized fluorophores that are non- or barely emissive.[25,46,58,63–68] Nevertheless compared with bioconjugates of other fluorescent labels such as the Dy68*x* and Dy67*x* series,[43] the bioconjugates of 6S-IDCC still reveal a promisingly high fluorescence quantum yield.

Origin of the IgG-Conjugated Dimers. The formation of H-type dimers in fluorophore-containing systems has been the subject of a multitude of studies addressing variations in quantities thought to be important in this process like dye hydrophobicity, linker length, size of transition dipole, delocalized charge, and symmetry.[12,69,70] Meanwhile, in addition to lanthanide chelate labels with their strongly Stokes-shifted emission,[44] even rare examples of multilabeled carriers like a Cy5-labeled mutant of the Cowpea mosaic virus have been reported, which allow dye-to-carrier (virus) ratios of 40 without a hint for fluorophore aggregation in the absorption spectra and thus, a linear enhancement in fluorescence intensity with increasing dye concentration.[71] This virus contains 60 cysteines as dye labeling sites at its surface separated by distances of 5.4 to 6.5 nm. This suggests that even for organic dyes with a considerable spectral overlap between absorption and emission like Cy5 known to form H-type aggregates, the use of multiple fluorescent reporters must not necessarily lead to fluorescence quenching if the dye–dye distances and dye orientation can be controlled and the formation of nonemissive aggregates acting as energy sinks for homo-FRET can be prevented. Moreover, in addition to dye–dye interactions, also dye–protein interactions have to be considered that can also alter the spectroscopic properties of fluorophores.[31]

We can only speculate about the reason for the formation of dimers at relatively low D/P ratios for such a hydrophilic nonaggregating dye like 6S-IDCC that communicates the close proximity of two or more dye molecules at the biomolecule in an orientation favorable for exciton coupling. Several explanations for such dye–dye interactions in fluorophore bioconjugates have been proposed in the literature and in previous studies from us ranging from dye adsorption, attachment of previously formed dimers, and cooperative dye binding to dye-induced protein aggregation.[43,67] The simplest case, adsorption of noncovalently bound fluorophore molecules can be commonly ruled out by proper purification procedures as employed here that have been previously validated by us for less hydrophilic dyes like Dy676, Dy681, and Dy682 using additional washing steps with buffer solutions containing deaggregating reagents like BSA or SDS.[43] Covalent attachment of dimers already formed in the reaction mixture used for biomolecule labeling can be most likely excluded for 6S-IDCC as well, as suggested by the minimum aggregation tendency of this dye and by absorption measurements of the reaction solution that did not provide a hint of dye aggregation. Alternatively, cooperative coupling may occur, favoring the attachment of a second dye molecule in the direct neighborhood of a lysine-bound fluorophore on the protein as is possible for statistical labeling of IgG with NHS esters.[25] Also protein aggregation enabling the interaction between

dx.doi.org/10.1021/bc4000349 | *Bioconjugate Chem.* 2013, 24, 1174–1185

fluorophores bound to different antibodies could account for the formation of H-type aggregates. Only recently, the aggregation behavior of conjugates of PEGylated and non-PEGylated indocyanine green ICG with anti-HER1 antibodies was investigated using size exclusion HPLC (SE-HPLC) and SDS-PAGE.[67] Here, the D/P-dependent formation of high molecular weight species, obviously aggregated proteins, was observed for antibodies labeled with non-PEGylated dye molecules, which was accompanied by the appearance of the typical H-type absorption bands. This could be prevented by PEGylation yielding nonaggregating dye bioconjugates that were stable in solution for several weeks without any spectroscopic evidence for dimer formation. Nevertheless, even the absorption spectra of the bioconjugates of the PEGylated ICG derivatives showed some hints for dye−dye interaction as suggested by the ratio of the intensities of the vibronic shoulder and the dye's main absorption band and the mismatch between the absorption spectra of the free and antibody-conjugated PEGylated fluorophores.[67]

Obviously, for the rational design of fluorophores that display maximum brightness in bioconjugates that contain more than a single dye, not only dye hydrophilicity and substituents favoring electrostatic and steric repulsion of the labels have to be considered and optimized but also the chemical nature, length, and position of the linker between the dye and the biomolecule. With this respect, the 6S-IDCC fluorophore seems to be superior to the Cy family. Here, however, more systematic studies with different biomolecules are needed to make sure that this observation holds true for a broad variety of proteins and antibodies with different dye-labeling sites and later also for DNA systems.

Functionality of Conjugates in Cellular Systems. Comparative cellular binding studies with the different bioconjugates shown in Table 2 and their targets were performed with confocal fluorescence microscopy and flow cytometry to address bioconjugate functionality and signal size under application-relevant conditions. For both Cy5.5 and 6S-IDCC conjugates of cetuximab, specific binding to the EGF receptor overexpressed in A431 cells was evident by fluorescence microscopy images of the cells incubated with these bioconjugates (see Figure 6, panels A−D and G) indicating preferential localization of these probes at the cell membrane where the EGF receptor is expressed (substantiated by a colocalization with a tight junction marker, Figure 6, panel G). Control experiments with the cell line A549 known to exhibit only weak EGFR expression (Figure 6, panel H, shown exemplarily for ctx−6S-IDCC) did not reveal binding of the targeted probes to these cell lines. Moreover, in addition, low intracellular signals are detectable, predominantly in the endosomal compartments, as a result of internalization of the dye bioconjugates by the EGF receptor after probe binding. Nonspecific IgG conjugates, which are often used as control samples for *in vivo* imaging studies, did not lead to cellular fluorescence. This also underlines the selectivity of our targeted probes.

For a more quantitative binding study and comparison of label and probe performance, we performed flow cytometric studies (FACS analysis) with the ctx and IgG conjugates of 6S-IDCC and Cy5.5 for all D/P ratios synthesized (see Table 2). The results, depicted in Figure 7, show that with increasing D/P ratio, a steadily enhanced cellular fluorescence results specific for the EGFR-positive A431 cells (upper panels). In the case of ctx−6S-IDCC (upper panel, right), the fluorescence intensity of

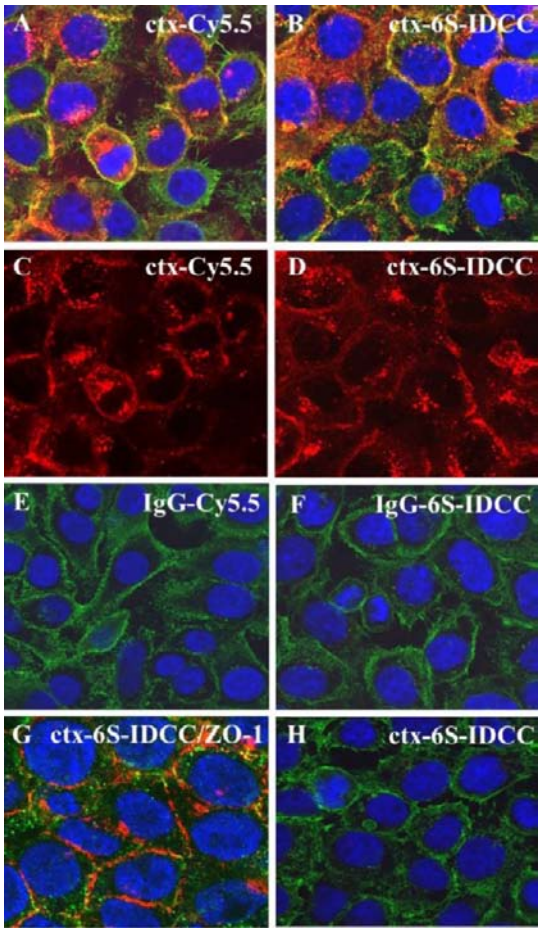

Figure 6. Confocal microscopy of A431 (A−G) and A549 (H) cells incubated for 45 min at 37 °C with ctx−Cy5.5, ctx−6S-IDCC, IgG−Cy5.5, or IgG−6S-IDCC (bioconjugates with D/P ratio of 1.3−1.4, red). In addition, the cells were stained with phalloidin−Alexa488 (cytoskeleton; A−F, H) or the tight junction marker ZO-1 (G, green). The nuclei were stained with DAPI (blue). Image acquisition was done with a 63× objective (A−F, H, green) or a 100× objective (G). C/D are identical to A/B with only the signal detected with the red channel being displayed.

the measured cells increased continuously with increasing D/P ratio, whereas for cells incubated with ctx−Cy5.5 (upper panel, left), dye bioconjugates with D/P ratios of 1.4 and 2.4 yielded similar signals (see curve 3 and 4) and no further gain in signal.

When the spectroscopic properties of the bioconjugates determined in PBS solution summarized in Table 2 and Table 3 are taken into account, the gain in fluorescence signal G_F resulting for the FACS measurements with the different bioconjugates can be estimated from the D/P ratio and the fluorescence quantum yields, Φ_f (see eq 3), thereby assuming identical molar absorption coefficients for the conjugated and free dyes and identical Φ_f values of the free and target-bound bioconjugates.

$$G_F = \frac{D/P(i+1) \times \Phi_f(i+1)}{D/P(i) \times \Phi_f(i)} \quad (3)$$

The experimental gain, G_E (eq 4), was determined from the mean fluorescence values of the FACS measurements (FL4; fluorescence intensity detected in the FL4 channel of the FACS instrument), see Table 3.

dx.doi.org/10.1021/bc4000349 | *Bioconjugate Chem.* 2013, 24, 1174−1185

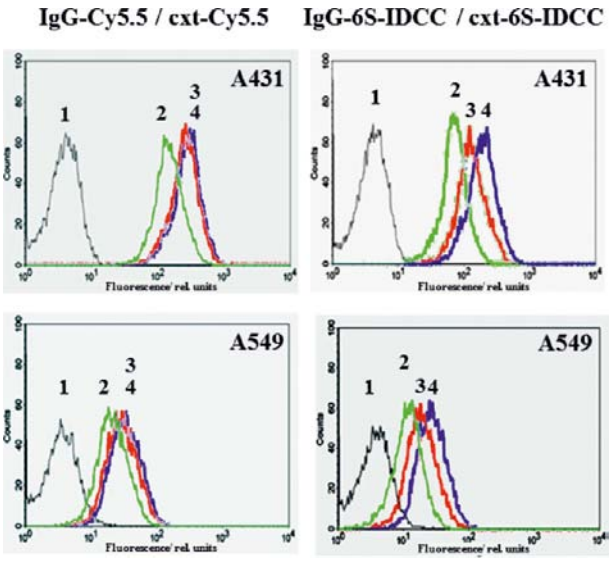

Figure 7. FACS analysis (excitation at 633 nm, detection with bandpass filter of 661 ± 8 nm) of viable, nonpermeabilized cells incubated with IgG−Cy5.5 or IgG−6S-IDCC conjugates with a D/P ratio of 1.3 (**1**) or with ctx−Cy5.5 conjugates with D/P ratios of 0.8 (**2**), 1.4 (**3**), and 2.4 (**4**) and ctx−6S-IDCC conjugates with D/P ratios of 0.6 (**2**), 1.3 (**3**), and 2.3 (**4**), respectively. The cell line A431 (upper panels) overexpresses EGFR, while A549 cells (lower panels) reveal a low EGFR expression, thus acting as control.

Table 3. FACS Analysis of A431 and A549 Cells with ctx−Cy5.5 and ctx−6S-IDCC Conjugates and Calculated and Experimentally Determined Fluorescence Gains in Correlation to the Spectroscopic Properties of These Conjugates

conjugate	D/P	Φ_f	calcd gain, G_F	mean FACS value (A431)	exptl gain, G_E (A431)	mean FACS value (A549)	exptl gain, G_E (A549)
ctx−Cy5.5	0.8	0.3		159		20	
ctx−Cy5.5	1.4	0.25	1.46	287	1.82	30	1.51
ctx−Cy5.5	2.4	0.16	1.10	302	1.05	34	1.15
ctx−6S-IDCC	0.6	0.29		75		9	
ctx−6S-IDCC	1.3	0.25	1.87	144	2.05	18	1.96
ctx−6S-IDCC	2.3	0.2	1.42	210	1.45	27	1.51

$$G_E = \frac{FL4(i+1)}{FL4(i)} \quad (4)$$

For both cell lines, the calculated and experimentally determined gains G_F and G_E agree very well. These calculations clearly reflect gain control by the fluorescence quantum yields of the bioconjugates. Accordingly, these data depict the superiority of the 6S-IDCC conjugates compared with the Cy5.5 conjugates as already detailed in the section on dye−antibody conjugates. Moreover, these data underline the potential of spectroscopic studies and accordingly derived signal-relevant optical properties of dye bioconjugates for the interpretation and understanding of results obtained with other fluorescence-based methods like FACS. The analogy found between the gains G_F and G_E suggests that the binding strength between the targeted probes and the EGF receptor at the cell membrane is independent of D/P ratio. However, this assumption has to be evaluated by a quantitative determination of the corresponding binding constants.

Interestingly, FACS experiments with A431 and A549 cells differing in EGFR expression level and our fluorophore−ctx conjugates revealed fluorescence signals for both cell lines and both ctx conjugates, although in the microscopic studies, we did not observe such signals for the latter cell line (see Figure 6, panel H). This underlines the superior detection sensitivity of FACS compared with CLSM. The ratios of the fluorescence intensities found for both cell lines in the FACS studies (mean FACS values; see Table 3, columns 5 and 7) are about 10:1 for A431 and A549 cells, for example, in the case of the ctx−6S-IDCC conjugates. Hence, the expression rate of the EGF receptors on the A549 cells can be estimated to be 10% of that on the A431 cells assuming a similar ligand−receptor affinity.

The cells incubated with ctx−Cy5.5 show higher fluorescence values than the cell incubated with ctx−6S-IDCC (Table 3, see rows 1−3 and rows 4−6) despite the comparable fluorescence quantum yields and molar absorption coefficient for a selected D/P ratio. This is related to the measurement conditions used for the FACS measurements, that is, an excitation wavelength of 633 nm and a bandpass filter of 661 ± 8 nm for fluorescence detection. The fluorescence signals of the ctx conjugates of both fluorophores, which reveal matching absorption spectra, are only weak in the spectral region between 653 and 669 nm, and the emission spectra of the ctx−6S-IDCC conjugates are 2 nm red-shifted in comparison to the emission bands of the ctx−Cy5.5 conjugates (Figure 8). As a result, less fluorescence can be collected in the case of the ctx−6S-IDCC conjugates.

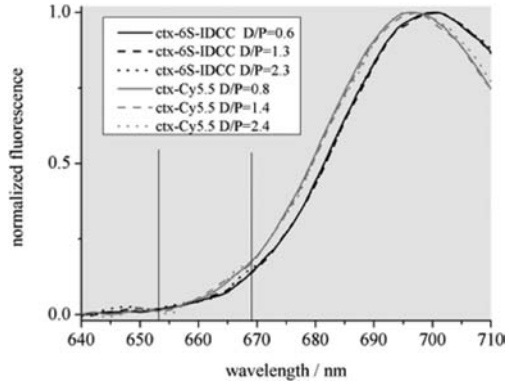

Figure 8. Normalized fluorescence spectra of the ctx−6S-IDCC and ctx−Cy5.5 conjugates. The corresponding absorption spectra (data not shown) match.

■ CONCLUSION AND OUTLOOK

We presented the spectroscopic properties of a series of new NIR-emissive fluorescent labels, the dyes 2S-IDCC, 4S-IDCC, and 6S-IDCC equipped with two, four, and six sulfonate groups, and the 6S-IDCC conjugates with the antibody cetuximab directed against the cancer-related EGF receptor and nonspecific IgG, including a comparison to the gold standard Cy5.5. This comparison underlines the strong influence of dye hydrophilicity on the aggregation behavior of these fluorophores in PBS and on the resulting fluorescence quantum yields. With 6S-IDCC, we could identify a very

dx.doi.org/10.1021/bc4000349 | Bioconjugate Chem. 2013, 24, 1174−1185

promising fluorescent label that reveals an even reduced aggregation tendency and higher molar absorption coefficients than Cy5.5 and a comparatively high fluorescence quantum yield in PBS. Conjugation of 6S-IDCC to cetuximab and IgG yielded conjugates with favorably high fluorescence quantum yields of 0.30, exceeding the fluorescence quantum yield of the free dye by 60%. Promisingly, for application-relevant low to medium D/P ratios between 0.5 and 3, the fluorescence quantum yields of the antibody conjugates of 6S-IDCC reached the values found for Cy5.5 conjugates. These data, in conjunction with the slightly higher molar absorption coefficient of 6S-IDCC, should provide the basis for higher signals and thus, enhanced detection sensitivities of optical probes utilizing this new label.

For the very hydrophilic dye 6S-IDCC, dye dimerization on the studied antibodies could be strongly reduced compared with its less hydrophilic derivatives and to other dyes like Cy5.5 and the Dy67*x* and Dy68*x* series previously studied by us and other examples from the literature. The minimum amount of dimers found for 6S-IDCC on cetuximab and IgG present the lowest values reported up to now for such simple labeling strategies (e.g., no PEGylated linker used), and this dimer fraction does not seem to be influenced by the type of antibody. Nevertheless, even for 6S-IDCC carrying six sulfonate groups, dimerization on proteins could not be completely prevented, underlining the need for a better understanding of the manifold origin of dye−dye interactions of biomolecule-conjugated fluorophores. In any case, our spectroscopic investigations and cellular binding studies clearly reveal that a high hydrophilicity is definitely a desirable property of a fluorescent label, although chemical approaches to impart a high hydrophilicity must not be necessarily restricted to the incorporation of sulfonate groups into the chromophore structure.

With the cellular binding studies performed here using fluorescence microscopy and fluorescence activated cell sorting, we could not only confirm the functionality of our ctx−6S-IDCC and ctx−Cy5.5-conjugates with respect to EGFR binding for all D/P ratios, but we could also demonstrate the direct correlation between the spectroscopic properties of such probes and the fluorescence signals resulting from FACS experiments. This also underlines the potential of a circumstantial spectroscopic study of dye−biomolecule conjugates for the prediction of the behavior of such systems in real-world fluorescence analysis in bioanalysis and clinical diagnostics and, thus, for dye screening and comparison.

AUTHOR INFORMATION

Corresponding Author

*Phone: 0049-30-8104 1134. Fax: 0049-30-8104 1157. E-mail: ute.resch@bam.de.

Notes

The authors declare no competing financial interest.

REFERENCES

(1) Lakowicz, J. R. (2006) *Principles of fluorescence spectroscopy*, 3rd ed., Springer Science+Business Media, LLC, New York.

(2) Valeur, B. (2002) *Molecular Fluorescence*, Wiley-VCH, Weinheim, Germany.

(3) Kossodo, S., Pickarski, M., Lin, S. A., Gleason, A., Gaspar, R., Buono, C., Ho, G. J., Blusztajn, A., Cuneo, G., Zhang, J., Jensen, J., Hargreaves, R., Coleman, P., Hartman, G., Rajopadhye, M., Duong, L. T., Sur, C., Yared, W., Peterson, J., and Bednar, B. (2010) Dual In Vivo Quantification of Integrin-targeted and Protease-activated Agents in Cancer Using Fluorescence Molecular Tomography (FMT). *Mol. Imaging Biol. 12*, 488−499.

(4) Resch-Genger, U., Grabolle, M., Cavaliere-Jaricot, S., Nitschke, R., and Nann, T. (2008) Quantum dots versus organic dyes as fluorescent labels. *Nat. Methods 5*, 763−775.

(5) Escobedo, J. O., Rusin, O., Lim, S., and Strongin, R. M. (2010) NIR dyes for bioimaging applications. *Curr. Opin. Chem. Biol. 14*, 64−70.

(6) Kobayashi, H., Ogawa, M., Alford, R., Choyke, P. L., and Urano, Y. (2010) New Strategies for Fluorescent Probe Design in Medical Diagnostic Imaging. *Chem. Rev. 110*, 2620−2640.

(7) Licha, K., and Resch-Genger, U. (2011) Probes for optical imaging: New developments. *Drug Discovery Today 8*, 87−94.

(8) Luo, S. L., Zhang, E. L., Su, Y. P., Cheng, T. M., and Shi, C. M. (2011) A review of NIR dyes in cancer targeting and imaging. *Biomaterials 32*, 7127−7138.

(9) Hermanson, G. T. (2008) *Bioconjugate Techniques*, 2nd ed., Elsevier, Amsterdam.

(10) Sperling, R. A., and Parak, W. J. (2010) Surface modification, functionalization and bioconjugation of colloidal inorganic nanoparticles. *Philos. Trans. R. Soc., A 368*, 1333−1383.

(11) Kobayashi, H., and Choyke, P. L. (2011) Target-Cancer-Cell-Specific Activatable Fluorescence Imaging Probes: Rational Design and in Vivo Applications. *Acc. Chem. Res. 44*, 83−90.

(12) Elias, D. R., Thorek, D. L. J., Chen, A. K., Czupryna, J., and Tsourkas, A. (2008) In vivo imaging of cancer biomarkers using activatable molecular probes. *Cancer Biomarkers 4*, 287−305.

(13) Mathejczyk, J. E., Pauli, J., Dullin, C., Resch-Genger, U., Alves, F., and Napp, J. (2012) High-sensitivity detection of breast tumors in vivo by use of a pH-sensitive near-infrared fluorescence probe. *J. Biomed. Opt. 17*, No. 076028.

(14) Lee, H., Akers, W., Bhushan, K., Bloch, S., Sudlow, G., Tang, R., and Achilefu, S. (2011) Near-Infrared pH-Activatable Fluorescent Probes for Imaging Primary and Metastatic Breast Tumors. *Bioconjugate Chem. 22*, 777−784.

(15) Sapsford, K. E., Tyner, K. M., Dair, B. J., Deschamps, J. R., and Medintz, I. L. (2011) Analyzing Nanomaterial Bioconjugates: A Review of Current and Emerging Purification and Characterization Techniques. *Anal. Chem. 83*, 4453−4488.

(16) Algar, W. R., Prasuhn, D. E., Stewart, M. H., Jennings, T. L., Blanco-Canosa, J. B., Dawson, P. E., and Medintz, I. L. (2011) The Controlled Display of Biomolecules on Nanoparticles: A Challenge Suited to Bioorthogonal Chemistry. *Bioconjugate Chem. 22*, 825−858.

(17) Mathejczyk, J. E., Pauli, J., Dullin, C., Napp, J., Tietze, L. F., Kessler, H., Resch-Genger, U., and Alves, F. (2011) Spectroscopically Well-Characterized RGD Optical Probe as a Prerequisite for Lifetime-Gated Tumor Imaging. *Mol. Imaging 10*, 469−480.

(18) Berezin, M. Y., Akers, W. J., Guo, K., Fischer, G. M., Daltrozzo, E., Zumbusch, A., and Achilefu, S. (2009) Long Fluorescence Lifetime Molecular Probes Based on Near Infrared Pyrrolopyrrole Cyanine Fluorophores for In Vivo Imaging. *Biophys. J. 97*, L22−L24.

(19) Louie, A. (2010) Multimodality Imaging Probes: Design and Challenges. *Chem. Rev. 110*, 3146−3195.

(20) Laux, E.-M., Behnke, T., Hoffmann, K., and Resch-Genger, U. (2012) Keeping particles brilliant - simple methods for the determination of the dye content of fluorophore-loaded polymeric particles. *Anal. Methods 4*, 1759−1768.

(21) Kovar, J. L., Simpson, M. A., Schutz-Geschwender, A., and Olive, D. M. (2007) A systematic approach to the development agents for optical imaging of mouse of fluorescent contrast cancer models. *Anal. Biochem. 367*, 1−12.

(22) Achilefu, S. (2004) Lighting up tumors with receptor-specific optical molecular probes. *Technol. Cancer Res. Treat. 3*, 393−409.

(23) Mujumdar, R. B., Ernst, L. A., Mujumdar, S. R., and Waggoner, A. S. (1989) Cyanine Dye Labeling Reagents Containing Isothiocyanate Groups. *Cytometry 10*, 11−19.

(24) Ballou, B., Fisher, G. W., Deng, J. S., Hakala, T. R., Srivastava, M., and Farkas, D. L. (1998) Cyanine fluorochrome-labeled antibodies

in vivo: Assessment of tumor imaging using Cy3, Cy5, Cy5.5, and Cy7. *Cancer Detect. Prev. 22*, 251−257.
(25) Gruber, H. J., Hahn, C. D., Kada, G., Riener, C. K., Harms, G. S., Ahrer, W., Dax, T. G., and Knaus, H. G. (2000) Anomalous fluorescence enhancement of Cy3 and Cy3.5 versus anomalous fluorescence loss of Cy5 and Cy7 upon covalent linking to IgG and noncovalent binding to avidin. *Bioconjugate Chem. 11*, 696−704.
(26) Mader, O., Reiner, K., Egelhaaf, H. J., Fischer, R., and Brock, R. (2004) Structure property analysis of petamethine indocyanine dyes: Identification of a new dye for life science applications. *Bioconjugate Chem. 15*, 70−78.
(27) Lisy, M. R., Goermar, A., Thomas, C., Pauli, J., Resch-Genger, U., Kaiser, W. A., and Hilger, I. (2008) In vivo near-infrared fluorescence imaging of carcinoembryonic antigen-expressing tumor cells in mice. *Radiology 247*, 779−787.
(28) Pauli, J., Vag, T., Haag, R., Spieles, M., Wenzel, M., Kaiser, W. A., Resch-Genger, U., and Hilger, I. (2009) An in vitro characterization study of new near infrared dyes for molecular imaging. *Eur. J. Med. Chem. 44*, 3496−3503.
(29) Pauli, J., Brehm, R., Spieles, M., Kaiser, W. A., Hilger, I., and Resch-Genger, U. (2010) Novel Fluorophores as Building Blocks for Optical Probes for In Vivo Near Infrared Fluorescence (NIRF) Imaging. *J. Fluoresc. 20*, 681−693.
(30) Busch, C., Schroter, T., Grabolle, M., Wenzel, M., Kempe, H., Kaiser, W. A., Resch-Genger, U., and Hilger, I. (2012) An In Vivo Spectral Multiplexing Approach for the Cooperative Imaging of Different Disease-Related Biomarkers with Near-Infrared Fluorescent Forster Resonance Energy Transfer Probes. *J. Nucl. Med. 53*, 638−646.
(31) Luschtinetz, F., Dosche, C., and Kumke, M. U. (2009) Influence of Streptavidin on the Absorption and Fluorescence Properties of Cyanine Dyes. *Bioconjugate Chem. 20*, 576−582.
(32) Povrozin, Y. A., Markova, L. I., Tatarets, A. L., Sidorov, V. I., Terpetschnig, E. A., and Patsenker, L. D. (2009) Near-infrared, dual-ratiometric fluorescent label for measurement of pH. *Anal. Biochem. 390*, 136−140.
(33) Povrozin, Y. A., Kolosova, O. S., Obukhova, O. M., Tatarets, A. L., Sidorov, V. I., Terpetschnig, E. A., and Patsenker, L. D. (2009) Seta-633-A NIR Fluorescence Lifetime Label for Low-Molecular-Weight Analytes. *Bioconjugate Chem. 20*, 1807−1812.
(34) Napp, J., Behnke, T., Fischer, L., Wuerth, C., Wottawa, M., Katschinski, D. M., Alves, F., Resch-Genger, U., and Schaeferling, M. (2011) Targeted Luminescent Near-Infrared Polymer-Nanoprobes for In Vivo Imaging of Tumor Hypoxia. *Anal. Chem. 83*, 9039−9046.
(35) Dmitriev, R. I., Zhdanov, A. V., Ponomarev, G. V., Yashunski, D. V., and Papkovsky, D. B. (2010) Intracellular oxygen-sensitive phosphorescent probes based on cell-penetrating peptides. *Anal. Biochem. 398*, 24−33.
(36) Eisfeld, A., and Briggs, J. S. (2006) The J- and H-bands of organic dye aggregates. *Chem. Phys. 324*, 376−384.
(37) Jelley, E. E. (1936) Spectral absorption and fluorescence of dyes in the molecular state. *Nature 138*, 1009−1010.
(38) Foerster, T., and Koenig, E. (1957) Absorptionsspektren und Fluoreszenzeigenschaften konzentrierter Loesungen organischer Farbstoffe. *Z. Elektrochem. 61*, 344−348.
(39) Buschmann, V., Weston, K. D., and Sauer, M. (2003) Spectroscopic study and evaluation of red-absorbing fluorescent dyes. *Bioconjugate Chem. 14*, 195−204.
(40) Luchowski, R., Matveeva, E. G., Gryczynski, I., Terpetschnig, E. A., Patsenker, L., Laczko, G., Borejdo, J., and Gryczynski, Z. (2008) Single Molecule Studies of Multiple-Fluorophore Labeled Antibodies. Effect of Homo-FRET on the Number of Photons Available Before Photobleaching. *Curr. Pharm. Biotechnol. 9*, 411−420.
(41) Luchowski, R., Sabnis, S., Szabelski, M., Sarkar, P., Raut, S., Gryczynski, Z., Borejdo, J., Bojarski, P., and Gryczynski, I. (2010) Self-quenching or uranin: Instrument response function for color sensitive photo-detectors. *J. Lumin. 130*, 2446−2451.
(42) Panchuk-Voloshina, N., Haugland, R. P., Bishop-Stewart, J., Bhalgat, M. K., Millard, P. J., Mao, F., Leung, W. Y., and Haugland, R. P. (1999) Alexa dyes, a series of new fluorescent dyes that yield exceptionally bright, photostable conjugates. *J. Histochem. Cytochem. 47*, 1179−1188.
(43) Pauli, J., Grabolle, M., Brehm, R., Spieles, M., Hamann, F. M., Wenzel, M., Hilger, I., and Resch-Genger, U. (2011) Suitable Labels for Molecular Imaging - Influence of Dye Structure and Hydrophilicity on the Spectroscopic Properties of IgG Conjugates. *Bioconjugate Chem. 22*, 1298−1308.
(44) Takalo, H., Mukkala, V. M., Mikola, H., Liitti, P., and Hemmila, I. (1994) Synthesis of europium(III) chelates suitable for labeling of bioactive molecules. *Bioconjugate Chem. 5*, 278−282.
(45) Matveeva, E. G., Terpetschnig, E. A., Stevens, M., Patsenker, L., Kolosova, O. S., Gryczynski, Z., and Gryczynski, I. (2009) Near-infrared squaraine dyes for fluorescence enhanced surface assay. *Dyes Pigm. 80*, 41−46.
(46) Schobel, U., Egelhaaf, H.-J., Brecht, A., Oelkrug, D., and Gauglitz, G. (1999) New donor−acceptor pair for fluorescent immunoassays by energy transfer. *Bioconjugate Chem. 10*, 1107−1114.
(47) Jue, R., Lambert, J. M., Pierce, L. R., and Traut, R. R. (1978) Addition of Sulfhydryl-groups to *Escherichia coli* Ribosomes by Protein Modification with 2-Iminothiolane (Methyl 4-mercaptobytyrimidate). *Biochemistry 17*, 5399−5406.
(48) Wuerth, C., Pauli, J., Lochmann, C., Spieles, M., and Resch-Genger, U. (2012) Integrating Sphere Setup for the Traceable Measurement of Absolute Photoluminescence Quantum Yields in the Near Infrared. *Anal. Chem. 84*, 1345−1352.
(49) Resch-Genger, U., Pfeifer, D., Monte, C., Pilz, W., Hoffmann, A., Spieles, M., Rurack, K., Hollandt, J., Taubert, D., Schonenberger, B., and Nording, P. (2005) Traceability in fluorometry: Part II. Spectral fluorescence standards. *J. Fluoresc. 15*, 315−336.
(50) Wuerth, C., Grabolle, M., Pauli, J., Spieles, M., and Resch-Genger, U. (2011) Comparison of Methods and Achievable Uncertainties for the Relative and Absolute Measurement of Photoluminescence Quantum Yields. *Anal. Chem. 83*, 3431−3439.
(51) Mujumdar, R. B., Ernst, L. A., Mujumdar, S. R., Lewis, C. J., and Waggoner, A. S. (1993) Cyanine Dye Labeling Reagents - Sulfoindocyanine Succinimidyl Esters. *Bioconjugate Chem. 4*, 105−111.
(52) Haughland, R. P. (1995) *Coupling of monoclonal antibodies with fluorophores*, Vol. *45*, Humana Press, Totowa, NJ.
(53) Hamann, F. M., Brehm, R., Pauli, J., Grabolle, M., Frank, W., Kaiser, W. A., Fischer, D., Resch-Genger, U., and Hilger, I. (2011) Controlled Modulation of Serum Protein Binding and Biodistribution of Asymmetric Cyanine Dyes by Variation of the Number of Sulfonate Groups. *Mol. Imaging 10*, 258−269.
(54) Berlier, J. E., Rothe, A., Buller, G., Bradford, J., Gray, D. R., Filanoski, B. J., Telford, W. G., Yue, S., Liu, J. X., Cheung, C. Y., Chang, W., Hirsch, J. D., Beechem, J. M., and Haugland, R. P. (2003) Quantitative comparison of long-wavelength Alexa Fluor dyes to Cy dyes: Fluorescence of the dyes and their bioconjugates. *J. Histochem. Cytochem. 51*, 1699−1712.
(55) Grabolle, M., Brehm, R., Pauli, J., Dees, F. M., Hilger, I., and Resch-Genger, U. (2012) Determination of the Labeling Density of Fluorophore-Biomolecule Conjugates with Absorption Spectroscopy. *Bioconjugate Chem. 23*, 287−292.
(56) Berlier, J. E., Rothe, A., Buller, G., Bradford, J., Gray, D. R., Filanoski, B. J., Telford, W. G., Yue, S., Liu, J. X., Cheung, C. Y., Chang, W., Hirsch, J. D., Beechem, J. M., Haugland, R. P., and Haugland, R. P. (2003) Quantitative comparison of long-wavelength Alexa Fluor dyes to Cy dyes: Fluorescence of the dyes and their bioconjugates. *J. Histochem. Cytochem. 51*, 1699−1712.
(57) Cox, W. G., Beaudet, M. P., Agnew, J. Y., and Ruth, J. L. (2004) Possible sources of dye-related signal correlation bias in two-color DNA microarray assays. *Anal. Biochem. 331*, 243−254.
(58) Schobel, U., Engelhaaf, H.-J., Fröhlich, D., Brecht, A., Oelkrug, D., and Gauglitz, G. (2000) Mechanism of fluorescence quenching in donor-acceptor labeled antibody conjugates. *J. Fluoresc. 10*, 147−154.
(59) Foerster, T. (1962) Elektronenspektren gekoppelter Moleküle. *Pure Appl. Chem. 4*, 121−134.

(60) Li, Q., and Pen, B. X. (1998) Benzimidazoloindocarbocyanines: Aggregation behavior, redox potential and photographic properties. *Dyes Pigm. 36*, 323−337.
(61) Zimmermann, H., and Scheibe, G. (1956) Zur Konstitution und Lichtabsorption der reversibel polymeren Form des Pseudoisocyanins. *Z. Elektrochem. 60*, 566−569.
(62) Sackett, D. L., and Wolff, J. (1987) Nile Red as a Polarity-Sensitive Fluorescent-Probe of Hydrophobic Protein Surfaces. *Anal. Biochem. 167*, 228−234.
(63) Dolghih, E., Roitberg, A. E., and Krause, J. L. (2007) Fluorescence resonance energy transfer in dye-labeled DNA. *J. Photochem. Photobiol., A 190*, 321−327.
(64) Johnson, J. R., Fu, N., Arunkumar, E., Leevy, W. M., Gammon, S. T., Piwnica-Worms, D., and Smith, B. D. (2007) Squaraine rotaxanes: Superior substitutes for Cy-5 in molecular probes for near-infrared fluorescence cell imaging. *Angew. Chem., Int. Ed. 46*, 5528−5531.
(65) Lavis, L. D., and Raines, R. T. (2008) Bright ideas for chemical biology. *ACS Chem. Biol. 3*, 142−155.
(66) Levitus, M., and Ranjit, S. (2011) Cyanine dyes in biophysical research: The photophysics of polymethine fluorescent dyes in biomolecular environments. *Q. Rev. Biophys. 44*, 123−151.
(67) Villaraza, A. J. L., Milenic, D. E., and Brechbiel, M. W. (2010) Improved Speciation Characteristics of PEGylated Indocyanine Green-Labeled Panitumumab: Revisiting the Solution and Spectroscopic Properties of a Near-Infrared Emitting anti-HER1 Antibody for Optical Imaging of Cancer. *Bioconjugate Chem. 21*, 2305−2312.
(68) Vira, S., Mekhedov, E., Humphrey, G., and Blank, P. S. (2010) Fluorescent-labeled antibodies: Balancing functionality and degree of labeling. *Anal. Biochem. 402*, 146−150.
(69) Packard, B. Z., Komoriya, A., Toptygin, D. D., and Brand, L. (1997) Structural characteristics of fluorophores that form intramolecular H-type dimers in a protease substrate. *J. Phys. Chem. B 101*, 5070−5074.
(70) Packard, B. Z., Komoriya, A., Nanda, V., and Brand, L. (1998) Intramolecular excitonic dimers in protease substrates: Modification of the backbone moiety to probe the H-dimer structure. *J. Phys. Chem. B 102*, 1820−1827.
(71) Soto, C. M., Blum, A. S., Vora, G. J., Lebedev, N., Meador, C. E., Won, A. P., Chatterji, A., Johnson, J. E., and Ratna, B. R. (2006) Fluorescent signal amplification of carbocyanine dyes using engineered viral nanoparticles. *J. Am. Chem. Soc. 128*, 5184−5189.